Waveform inversion by model reduction using spline interpolation

Guillaume Barnier, Ettore Biondi, and Robert G. Clapp, Stanford University*

SUMMARY

We investigate the use of model reduction by interpolation for improving the convergence to the true solution of full waveform inversion (FWI) techniques. We develop a 2D spline interpolation workflow using basic spline (B-spline) functions that allows us to represent our unknown model parameters on a coarser nonuniform grid. We propose a new FWI workflow where all data are simultaneously inverted, but the spline grid is gradually refined with iterations. The inverted model for a given grid is then used as the initial guess for the following inversion performed with a finer grid. We test our proposed workflow on the Marmousi model. We find that when FWI converges to the true solution, our proposed method recovers the same solution. The conventional frequency continuation or data-domain multi-scale approach can therefore be substituted by a model-space multi-scale one, where the wavenumber content of the updates are controlled by the rate of refinement of the spline grid. In addition, we analyze the necessity of low frequencies within the acquired data when a L2-norm data-misfit function is employed. We find that when the acquired data lack low-frequency content, both data- and model-domain multi-scale approaches converge to local minima.

INTRODUCTION

FWI has the ability of simultaneously recovering all model wavelengths or scales without making any limiting modeling or data assumptions, such as ray approximation or recording of primary reflections only, when setting the inverse problem (Tarantola, 1984). However, one of the main drawbacks associated to this approach is its inability of providing the correct or true model when an inaccurate starting guess is provided to any FWI workflow, usually referred to as cycle skipping (Virieux and Operto, 2009).

Many data- and model-space techniques have been proposed over the last two decades to mitigate this issue. Some of these methods attempt to solve the problem by extending the number of model parameters used during the inversion (Van Leeuwen and Herrmann, 2013; Yao et al., 2014; Biondi and Almomin, 2014; Huang and Symes, 2015); whereas, others try to modify the data term to ameliorate the convergence of FWI (Metivier et al., 2016; Warner and Guasch, 2016; Li and Demanet, 2016). The mathematical concept behind all of these approaches is related to the convexification of the FWI objective function (Barnier et al., 2018). For example, it has been observed that the extent of the basin of attraction towards the global minimum increases when the low-frequency content of the data is inverted (Bunks et al., 1995; Fichtner, 2010). As a matter of fact, low-frequency sources specifically designed for FWI have been proposed and tested for exploration purposes (Dellinger et al., 2016).

Mora (1989) shows the connection between the propagation direction of the source and receiver wavefields and the wavenumber updates introduced by their cross-correlation (i.e., the model scale that is updated at each iteration). Sirgue and Pratt (2004) extend this discussion and describe the connection between the data frequency content and the model updates and propose a method to select the frequency band to be inverted. Based on the fact that the frequency content of the data will update certain wavenumber components of the model, we describe a method in which the entire bandwidth of the data is simultaneously inverted but we limit the wavenumbers or scales of the model by using a B-spline representation (De Boor, 1986; Shene, 2011). We follow the same update strategy of the data-space multi-scale approach in which the inversion procedure starts by inverting low frequencies and gradually increases the data bandwidth as the inversion progresses (Bunks et al., 1995). In fact, we start our inversion method by inverting the low-wavenumber components of the model by placing the spline nodes on a coarse grid, and we gradually increase the model scales by refining the spline node positions to a denser grid.

We compare the data- and model-space multi-scale approaches on the Marmousi model (Martin et al., 2006) in which acoustic pressure data are generated, and a v(z) model is used as initial guess. We inverted two datasets with different frequency contents, one in which low frequencies are present and one in which they are missing. For the first scenario, we show that simultaneous data inversion (i.e., without adopting any multi-scale approach) cannot retrieve an accurate model, while both multi-scale approaches converge to a similar correct solution. When the low frequency energy is missing, neither method could retrieve the true model. Finally, we analyze the wavenumber spectra of the model updates, stemming from the tested inversions, and show that one potential key factor for the success of a FWI method is the retrieval of the low-wavenumber components of the model at early stages of the inversion.

METHODOLOGY

In this section we describe our interpolation implementation using B-spline functions, and how we employ them in our proposed FWI scheme.

Interpolation using B-spline functions

B-spline functions are commonly used in computer-aided design and graphic to draw smooth curves and surfaces passing in the vicinity of a set of control points. These functions can hence be used to interpolate coarsely sampled points to a finer grid when we do not require to fit the control points exactly. Here, the control points correspond to our unknown model parameters on a coarse grid $\mathbf{m}_c$, and the interpolation linearly maps these points to the finite-difference (finer) propagation grid $\mathbf{m}_f$. In 2D, the mapping is given by the following equation (Shene, 2011),

$$\mathbf{m}_f = \sum_{i=0}^{N_z^c} \sum_{j=0}^{N_x^c} N_{i,k} N_{j,k} \mathbf{m}_c, \tag{1}$$

where $N_{i,k}$ and $N_{j,k}$ are the B-spline functions of order k for the z- and x-directions, respectively. N_z^c and N_x^c are the number of unknown parameters (control points) on the coarse grid for each direction. Though the coarse grid must be parametrized on a net, each direction does not need to be arranged uniformly, which allow us to adapt the spline nodes sampling density according to geological features. Moreover, B-spline functions have very limited support which makes the interpolation cost quite attractive, even in 3D. We use $k = 3$, implying continuity of the interpolated function up to the second-order derivative.

Model-space multi-scale approach

The conventional FWI objective function is given by the following equation:

$$\phi(\mathbf{m}_f) = \frac{1}{2} \left\| \mathbf{f}(\mathbf{m}_f) - \mathbf{d}_{obs} \right\|_2^2, \tag{2}$$

where $\mathbf{m}_f$ is the velocity model represented on the finite-difference grid, $\mathbf{d}_{obs}$ is the observed data, and $\mathbf{f}$ is the modeling operator. In our proposed model-space multi-scale approach, we represent the velocity model on a coarse grid that is then mapped into a finer finite-difference one. Therefore, we modify equation 2 to the following:

$$\phi(\mathbf{m}_c) = \frac{1}{2} \left\| \mathbf{f}(\mathbf{S}\mathbf{m}_c) - \mathbf{d}_{obs} \right\|_2^2, \tag{3}$$

where $\mathbf{m}_c$ is the coarse-grid model parameters, and $\mathbf{S}$ is the interpolation operator constructed using equation 1. The initial coarse-grid model $\mathbf{m}_c$ for a given inversion is obtained by applying the pseudo-inverse operator $\mathbf{S}^\dagger$ to a model defined on a fine grid.

NUMERICAL EXAMPLE

We compare our proposed methodology with the conventional data-space multi-scale approach on the Marmousi model (Martin et al., 2006) (Figure 2(a)). We generate noise-free pressure data with a two-way acoustic modeling operator. We test two scenarios, one where unrealistic low frequencies below 2 Hz are present (scenario 1), and one with no energy below 4 Hz (scenario 2). Figure 1(a) and (b) show the wavelet spectra used for all our FWI workflows. Our model multi-scale approach is conducted by simultaneously inverting the last bandwidth of the conventional data-space approach (blue curves in Figures 1(a) and (b)). For all the tested inversions, we start with the same initial v(z) velocity model shown in Figure 2(b).

Broadband data inversion

Figure 2(c) shows the inverted model after conducting a data-space multi-scale approach using all frequency bands displayed

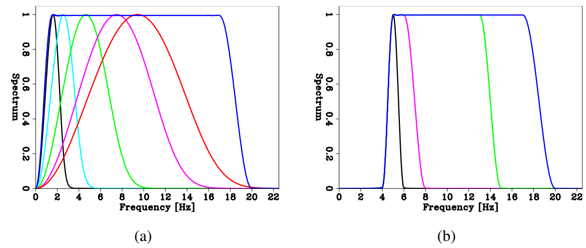

Figure 1: Set of wavelet spectra used for the FWI workflows. (a) Set of wavelet spectra used for the data-space multi-scale FWI of scenario 1. (b) Set of wavelet spectra used for the data-space multi-scale FWI of scenario 2. In each figure, the blue curve corresponds to both the last frequency band used in the data-space approach as well as the frequency band used in the model-space approach.

in Figure 1(a). As expected, the recovered model is accurate. Figure 2(d) shows the inverted model obtained by simultaneously inverting the full bandwidth (blue curve in Figure 1(a)) without adopting a multi-scale approach. Even with the presence of low-frequency energy, the inversion converged to a local minimum, which is much more inaccurate than the one obtained with the data-space multi-scale approach.

Figure 3 shows the spline grid arrangement (magenta dots overlaid on top of the true model) used for our first step of model-space multi-scale approach. We start with a horizontal node spacing of 5 km, and vertical spacing of 1 km in the sediments. In the vicinity of the water bottom, we use a finer vertical spacing (200 m) to account for the sharp interface (the only prior geological information we assume). We conduct our model-space multi-scale approach by inverting the full bandwidth for a sequence of six spline arrangements. We use the output of an inversion for one arrangement as the initial model for the next (finer) one. The panels in Figure 4 show the inverted models for the last four spline arrangements. The final inverted model is shown in Figure 4(d) and was obtained by using the same uniform sampling as for the finite-difference propagation grid (20 m in both directions). Both data- and model-space multi-scale methods converge to a similar velocity model (Figures 2(c) and 4(d)), which are quite accurate. The model-space multi-scale inverted model is slightly smoother since the spline interpolation enforces continuity of the interpolated function and of its derivatives up to the order employed.

Cycle-skipped Marmousi

We remove all the energy below 4 Hz in the recorded data (Figure 1(b)). By doing so, we create a more realistic data bandwidth and we make any FWI method more likely to converge to a local minimum given the inaccurate v(z) starting model. For the data-space multi-scale approach, we use four width-increasing bands shown in Figure 1(b). In the model-space counterpart, we employ the same spline refinement schedule as in scenario 1. The final inverted models for each scheme are shown in Figure 5. This example shows the already noticed duality between the frequency content of the data and the updates that will be generated during any inversion scheme (Sir-

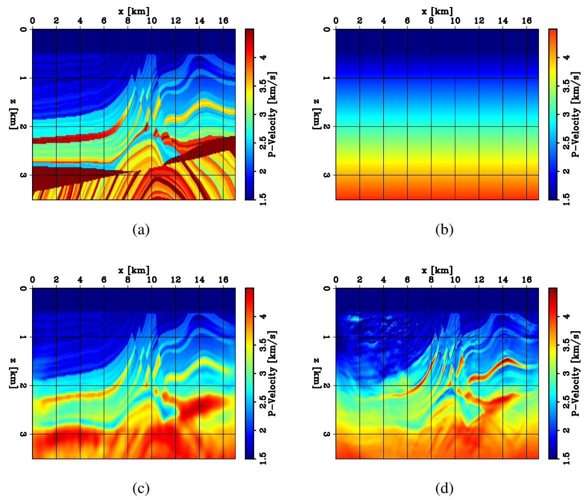

Figure 2: (a) True subsurface Marmousi model. (b) Initial v(z) velocity model used in all tests. (c) Inverted model conducted with a data-space multi-scale FWI using the sequence of frequency bands shown in Figure 1(a). (d) FWI model obtained by simultaneously inverting the entire data bandwidth (blue curve in Figure 1(a)).

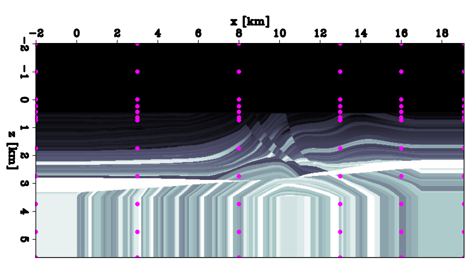

Figure 3: First spline mesh used. The magenta dots represent the B-spline nodes of the first model-space multi-scale FWI. For reference, the true velocity including the padding of the absorbing boundaries is displayed in the background.

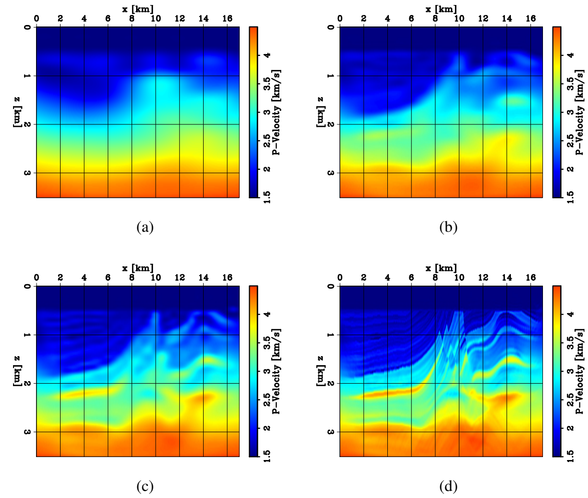

Figure 4: Inverted models using model-space multi-scale FWI for the last four refinement steps of our workflow. (a) $dz = 0.2$ km, $dx = 2$ km, (b) $dz = 0.1$ km, $dx = 1$ km, (c) $dz = 0.08$ km, $dx = 0.5$ km, and (d) $dz = 0.02$ km, $dx = 0.02$ km.

gue and Pratt, 2004). In fact, in both cases, the inversions converge to inaccurate similar solutions (i.e., the data- and model-space multi-scale methods may have similar objective-function shapes).

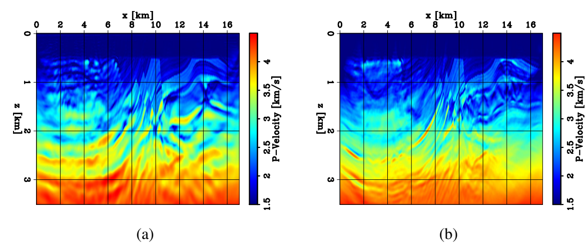

Figure 5: Inverted models for scenario 2. (a) Final inverted model using the data-space approach. (b) Final inverted model using the model-scale approach.

Wavenumber spectrum analysis

We analyze the wavenumber spectra of the model updates obtained in all the tested inversions. To obtain these spectra, we subtract the initial velocity model from the inverted one and apply a 2D Fourier transform.

Figure 5 displays the various spectra obtained from the previous examples. The top panels respectively show the update spectra for the data-space (left) and model-space (right) multi-scale approach for scenario 1. In the same order, the bottom panels show the analogous update spectra but for scenario 2. The central panel shows the ideal update spectrum (i.e., spectrum of the true model in which the starting model is subtracted). The inversion-related panels are computed on inverted model at the second stage of both data- and model-space multi-scale approaches (i.e., the low frequencies and wavenumbers are expected to be inverted). In the two case, when the multi-scale methods converged to a satisfactory result, we can observed that both schemes first retrieve the low-wavenumber component of the model that are clearly missing from the starting model (Figure 6(c)). On the other hand, when the low-frequency content of the data is missing, both approaches fail to fill that part of the model spectrum. This observation has already been noticed by different authors that proposed to enhance the low-wavenumber component of the gradient at early stage of any FWI algorithm (Xu et al., 2012; Zhou et al., 2015). Here, we show a numerical example in which this fact seems critical for the success of the FWI method. However, it is still mathematically unclear why that portion of the spectrum plays such an important role.

CONCLUSIONS

We describe a model-space multi-scale FWI workflow that may be used as an alternative approach to the conventional data-domain multi-scale scheme. The entire data bandwidth is injected and simultaneously inverted; however, the wavenumber content of the model updates is controlled by the arrangement of spline nodes distributed on a coarse grid. As the inversion progresses, we gradually refine the density of our spline grid to allow for higher wavenumber updates into the model.

We present two synthetic examples in which we invert acoustic data generated using the Marmousi model. We show that when low-frequency content is recorded, both data- and model-space multi-scale methods provide a similar correct inverted model, while a simultaneous data inversion fails to provide the correct one. In the second example we invert a dataset where no energy below 4 Hz is recorded. In this case, neither multi-scale methods succeed to invert the correct model. We compare the wavenumber spectra of the model updates of the two tests and show that, when FWI converges, the one of the fundamental factor seems to be related to the inversion of the low-wavenumber model component at early stages of the inversion.

This model parametrization allows the crucial low-wavenumber updates to be retrieved at early inversion stages from all components of the data without manually selecting specific events (e.g., refractions or reflections). Therefore, its applications may include all tomographic velocity-model building techniques based on reflection data.

ACKNOWLEDGMENTS

We would like to thank the Stanford Exploration Project affiliate companies for financial support.

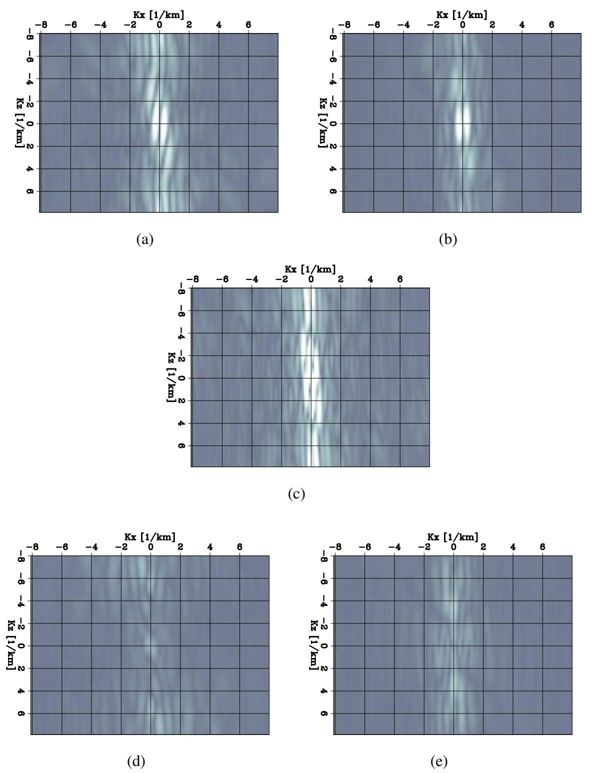

Figure 6: Wavenumber spectra of the model updates (i.e., spectra of inverted models in which the initial one is subtracted) for the second band of each multi-scale approach. The top two panels, (a) and (b), show the data- and model-space multi-scale spectrum updates for the data in which low frequencies are recorded (scenario 1), respectively. The middle panel (c) is the ideal or true spectrum update (i.e., true model minus the initial one). The bottom panels (d) and (e) show the analogous spectra as (a) and (b) but for scenario 2.

REFERENCES

Barnier, G., E. Biondi, and B. Biondi, 2018, Full waveform inversion by model extension: 88th Annual International Meeting, SEG, Expanded Abstracts, 1183–1187, doi: https://doi.org/10.1190/segam2018-2998613.1.

Biondi, B., and A. Almomin, 2014, Simultaneous inversion of full data bandwidth by tomographic full-waveform inversion: Geophysics, **79**, no. 3, WA129–WA140, doi: https://doi.org/10.1190/geo2013-0340.1.

Bunks, C., F. M. Saleck, S. Zaleski, and G. Chavent, 1995, Multiscale seismic waveform inversion: Geophysics, **60**, 1457–1473, doi: https://doi.org/10.1190/1.1443880.

De Boor, C., 1986, B(asic)-spline basics: Technical report, Wisconsin Univ-Madison Mathematics Research Center.

Dellinger, J., A. Ross, D. Meaux, A. Brenders, G. Gesoff, J. Etgen, J. Naranjo, G. Openshaw, and M. Harper, 2016, Wolfspar, an FWI-friendly ultralow-frequency marine seismic source: 88th Annual International Meeting, SEG, Expanded Abstracts, 4891–4895, doi: https://doi.org/10.1190/segam2016-13762702.1.

Fichtner, A., 2010, Full seismic waveform modelling and inversion: Springer Science and Business Media.

Huang, Y., and W. W. Symes, 2015, Born waveform inversion via variable projection and shot record model extension: 85th Annual International Meeting, SEG, Expanded Abstracts, 1326–1331, doi: https://doi.org/10.1190/segam2015-5870371.1.

Li, Y. E., and L. Demanet, 2016, Full-waveform inversion with extrapolated low-frequency data: Geophysics, **81**, no. 6, R339–R348, doi: https://doi.org/10.1190/geo2016-0038.1.

Martin, G. S., R. Wiley, and K. J. Marfurt, 2006, Marmousi2: An elastic upgrade for Marmousi: The Leading Edge, **25**, 156–166, doi: https://doi.org/10.1190/1.2172306.

Metivier, L., R. Brossier, E. Oudet, Q. Me rigot, and J. Virieux, 2016, An optimal transport distance for full-waveform inversion: Application to the 2014 chevron benchmark data set: 86th Annual International Meeting, SEG, Expanded Abstracts, 1278–1283, doi: https://doi.org/10.1190/segam2016-13870096.1.

Mora, P., 1989, Inversion= migration+ tomography: Geophysics, **54**, 1575–1586, doi: https://doi.org/10.1190/1.1442625.

Shene, C.-K., 2011, Introduction to computing with geometry notes.

Sirgue, L., and R. G. Pratt, 2004, Efficient waveform inversion and imaging: A strategy for selecting temporal frequencies: Geophysics, **69**, 231–248, doi: https://doi.org/10.1190/1.1649391.

Tarantola, A., 1984, Inversion of seismic reflection data in the acoustic approximation: Geophysics, **49**, 1259–1266, doi: https://doi.org/10.1190/1.1441754.

Van Leeuwen, T., and F. J. Herrmann, 2013, Mitigating local minima in full-waveform inversion by expanding the search space: Geophysical Journal International, **195**, 661–667, doi: https://doi.org/10.1093/gji/ggt258.

Virieux, J., and S. Operto, 2009, An overview of full-waveform inversion in exploration geophysics: Geophysics, **74**, no. 6, WCC1–WCC26, doi: https://doi.org/10.1190/1.3238367.

Warner, M., and L. Guasch, 2016, Adaptive waveform inversion: Theory: Geophysics, **81**, no. 6, R429–R445, doi: https://doi.org/10.1190/geo2015-0387.1.

Xu, S., D. Wang, F. Chen, Y. Zhang, and G. Lambare, 2012, Full waveform inversion for reflected seismic data: 74th Annual International Conference and Exhibition Incorporating EUROPEC, EAGE, Extended Abstracts, doi: https://doi.org/10.3997/2214-4609.20148725.

Yao, G., M. Warner, and A. Silverton, 2014, Reflection FWI for both reflectivity and background velocity: 76th Annual International Conference and Exhibition, EAGE, Extended Abstracts, doi: https://doi.org/10.3997/2214-4609.20141089.

Zhou, W., R. Brossier, S. Operto, and J. Virieux, 2015, Full waveform inversion of diving and reflected waves for velocity model building with impedance inversion based on scale separation: Geophysical Journal International, **202**, 1535–1554, doi: https://doi.org/10.1093/gji/ggv228.